

ture encloses the center of the core and its immediate surroundings. In this region, of course, the simple spiral representation of isointensity lines is not applicable.

Our experimental evidence for the existence and the structure of the core of the spiral pattern exhibited in the BZ reaction system shows the importance of a locally restricted phenomenon driving and controlling the spiral propagation through space. Our observation shows the stable coexistence of two different dynamic states in space. Further application of the digital video technique for a quantitative description of the dynamic behavior of the core and the local predominance of specific reaction steps at its center is expected to lead to stimulating contributions to our knowledge of chemical waves. Furthermore, the spatial transition from the local to the bulk state in terms of the outward moving chemical activity is of utmost interest.

References and Notes

1. C. Vidal and A. Pacault, Eds., *Springer Ser. Synerget.* **27**, 1 (1984). See also vols. 6, 12, 19, and 28 in this series.
2. H.-G. Busse, *J. Phys. Chem.* **73**, 750 (1969); A. N. Zaikin and A. M. Zhabotinskii, *Nature (London)* **225**, 535 (1970); H.-G. Busse and B. Hess, *ibid.* **244**, 203 (1973).
3. A. T. Winfree, *Science* **175**, 634 (1972); *Sci. Am.* **230**, 82 (June 1974).
4. R. J. Field, E. Körös, R. M. Noyes, *J. Am. Chem. Soc.* **94**, 8649 (1972); L. Bornmann, H.-G. Busse, B. Hess, *Z. Naturforsch. Teil B* **28**, 93 (1973); *Z. Naturforsch. Teil C* **28**, 514 (1973); L. Bornmann *et al.*, *Z. Naturforsch. Teil B* **28**, 824 (1973).
5. K. Showalter, R. M. Noyes, H. Turner, *J. Am. Chem. Soc.* **101**, 7463 (1979); M. L. Smoes, *Springer Ser. Synerget.* **6**, 80 (1980).
6. P. M. Wood and J. Ross, *J. Chem. Phys.* **82**, 1924 (1985).
7. P. Ortoleva and J. Ross, *ibid.* **58**, 5673 (1973); J. J. Tyson, *Lect. Notes Biomath.* **10**, 1 (1976); P. C. Fife, *NATO Adv. Study Inst. Ser. B* **116**, 371 (1984).
8. S. C. Müller and T. Plesser, *Lect. Notes Biomath.* **55**, 246 (1984).
9. _____, B. Hess, *Anal. Biochem.* **146**, 125 (1985).
10. Because of the curvature of the TV observation screen, the geometry of the photographs in Figs. 1, 2, and on the cover is slightly distorted.
11. We thank K. Dreher, U. Heidecke, B. Plettenberg, R. Schüller, and G. Schulte for skillful technical and programming support.

23 April 1985; accepted 12 July 1985

Intracellular Free Calcium Localization in Neutrophils During Phagocytosis

Abstract. *Intracellular free calcium (Ca^{2+}_i) is thought to be an important second messenger for phagocyte functions. The fluorescent indicator Quin2 was used to measure and visualize $[Ca^{2+}]_i$ in human neutrophils during chemotaxis toward, and phagocytosis of, opsonized zymosan. In neutrophils migrating toward zymosan, $[Ca^{2+}]_i$ was highest in the lamellipodium. Neutrophils ingesting opsonized zymosan had the highest $[Ca^{2+}]_i$ in the pseudopods and periphagosomal cytoplasm. Most of the increase in $[Ca^{2+}]_i$ was from extracellular sources. Regional increments in $[Ca^{2+}]_i$ are strategically located to modulate such cellular functions as chemotaxis, oxidative activity, and degranulation.*

DANIEL W. SAWYER
JAMES A. SULLIVAN
GERALD L. MANDELL*

*Division of Infectious Diseases,
Department of Internal Medicine,
University of Virginia School
of Medicine, Charlottesville 22908*

* To whom correspondence should be addressed.

Intracellular free calcium (Ca^{2+}_i) is thought to be an important secondary messenger for many phagocyte functions including chemotaxis (1), phagocytosis (2), and degranulation (3). Surface stimuli trigger transient changes in calcium concentration that are associated with these effector functions. The subcellular pattern of Ca^{2+} distribution in resting and stimulated neutrophils is largely unknown because in prior studies changes in populations of cells were analyzed with fluorometric or photometric techniques. We investigated the alterations in the subcellular distribution of Ca^{2+} in

neutrophils during chemotaxis and phagocytosis with the Ca^{2+} indicator Quin2. This indicator emits Ca^{2+} -dependent fluorescence when excited at 340 nm and Ca^{2+} -independent fluorescence when excited at 360 nm (4).

Neutrophils were isolated from heparinized (10 units per milliliter) venous blood of normal volunteers by Ficoll-Hypaque separation (5); after isolation, the neutrophils were subjected to dextran sedimentation and hypotonic lysis of erythrocytes. Isolated neutrophils were washed with Hanks balanced salt solution (HBSS) and loaded with 25 μ M Quin2 ester (Calbiochem) for 60 minutes at 37°C. The cells were washed with HBSS plus 1 percent autologous heat-inactivated serum and incubated at 24°C for 120 minutes, allowing hydrolysis of the ester to the active Ca^{2+} indicator. For experiments without extracellular calcium ($[Ca^{2+}]_0$), the Quin2-loaded cells were spun and resuspended in Ca^{2+} - and Mg^{2+} -free HBSS with 10 mM EGTA.

Quin2-loaded neutrophils (10^6 cells per milliliter) were transferred to a cover glass, mixed with opsonized zymosan (6), and observed with a microscope (Leitz Orthoplan) equipped with a 100-W mercury vapor epi-illuminator, quartz optical elements in the epifluorescence pathway, and a glycerine immersion objective (Nikon 100 \times UV-CF). Neutrophils for analysis were selected with bright-field microscopy. Images of Quin2-loaded neutrophils were collected with a silicon-intensified target camera (DAGE series 65) and stored for later processing with an image processor (Quantex 9210). Three images of single cells were collected in sequence over less than 5 seconds. The first image was a processed bright-field image based on the use of a modification of asymmetric illumination contrast optics (7), in which a circular filter (50 mm in diameter), one half clear and one half black, was placed in the transmitted light path. Processing included the averaging of eight frames, background subtraction, and gray-scale expansion. This image was used to establish the location of morphological features. The second and third images were fluorescence images obtained with a long-pass barrier filter that transmits wavelengths >475 nm. Cells were excited first at 340 nm (10-nm half width) and subsequently at 360 nm (10-nm half width paired with a .25 percent transmission neutral density filter). Each of the fluorescence images was an average of eight video frames. The two fluorescence images were separated in time by less than 0.5 second.

To determine $[Ca^{2+}]_i$, we first converted each raw fluorescence image to a pixel array (640 by 480 by 8 bits). Point density readings were taken first within the 360-nm fluorescence image, and then at the corresponding pixels within the 340-nm fluorescence image. The ratio of the fluorescence intensity at 340 nm to that at 360 nm, when applied to a curve relating known concentrations of Ca^{2+} (8, 9), indicated the $[Ca^{2+}]_i$ at that point in the cell. We did not detect neutrophil autofluorescence with this system.

To visually display the relative local $[Ca^{2+}]_i$ within a single cell, we converted the intensity of each pixel of the two digitized fluorescence images to a logarithm and subtracted the 360-nm log image from the 340-nm log image. The antilog of the difference represents the free Ca^{2+} distribution and is independent of Quin2 concentrations at specific image locations.

Measurements of $[Ca^{2+}]_i$ in unstimulated but polarized neutrophils are listed in Table 1A. The mean $[Ca^{2+}]_i$ in the

front third of these cells (the lamellipodium) was not significantly different from the $[Ca^{2+}]_i$ in the middle third of the cell (the cell body). A computer-enhanced image of an asymmetrically illuminated cell is shown in Fig. 1A. The nearly simultaneous monochrome and color-coded ratio images are shown in Fig. 1, B and C, respectively. Free cytoplasmic Ca^{2+} is evenly distributed in these cells.

In contrast, the mean $[Ca^{2+}]_i$ in the lamellipodium of stimulated neutrophils migrating toward opsonized zymosan particles was significantly greater than the $[Ca^{2+}]_i$ in the cell body by 37.8 ± 16 nM (Table 1B). Figure 1D shows a neutrophil approaching an opsonized zymosan particle.

Figure 1, E and F, shows the monochrome and color-coded ratio images of the same cell. The red area has the

highest $[Ca^{2+}]_i$. The lamellipodium was the region of highest free cytosolic Ca^{2+} . Other studies have shown this to be a region of high F-actin, actin-binding proteins, and myosin (10). Stossel *et al.* (11) postulated that neutrophil movement occurs subsequent to growth of the actin network, resulting from a regional decrease in $[Ca^{2+}]_i$. Although we found that $[Ca^{2+}]_i$ is increased in the lamellipodium, it is possible that there is a region

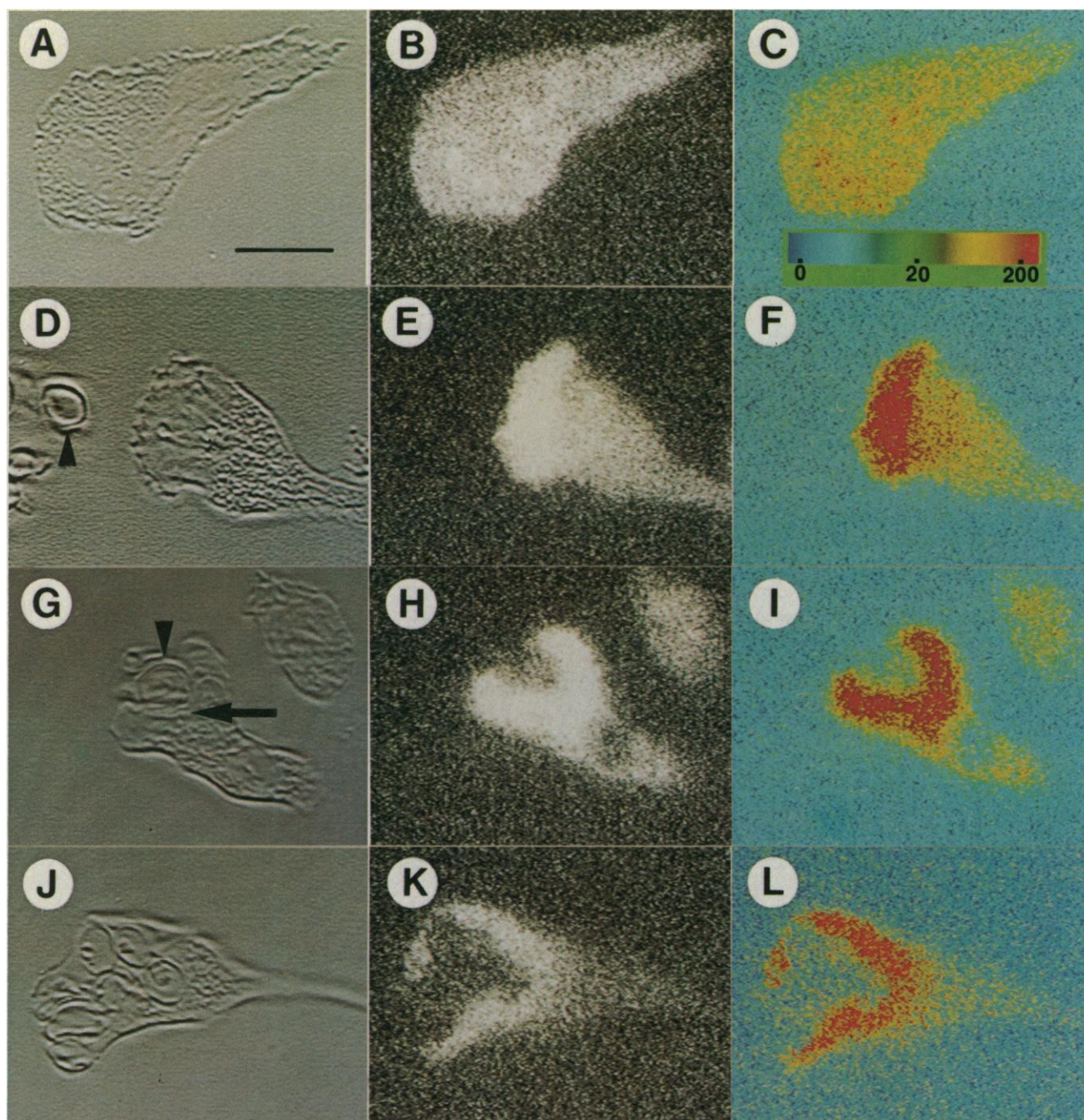


Fig. 1. Subcellular free calcium distribution. (A) Computer-enhanced, asymmetrically illuminated bright-field image of an unstimulated neutrophil that is polarized (has an identifiable head and tail). Bar, 10 μ m. (B) Monochrome ratio image showing the $[Ca^{2+}]_i$ distribution. The white area represents the highest $[Ca^{2+}]_i$ and black the lowest $[Ca^{2+}]_i$. (C) Color-coded ratio image of the same cell as in (B). The numbers in the bar reflect nanomolar concentrations of $[Ca^{2+}]_i$. (D) Neutrophil migrating toward an opsonized zymosan particle (arrowhead). (E and F) Monochrome and color-coded ratio images of the same cell as in (D). (G) Neutrophil with pseudopods surrounding an opsonized zymosan particle. The arrow indicates the developing periphagosomal cytoplasm. (H and I) Ratio images of the same cell as in (G). (J through L) Images showing a neutrophil that has ingested several zymosan particles.

at the very edge of the leading front with a low $[Ca^{2+}]_i$.

Phagocytosis of particles stimulates numerous cellular responses, including oxidative activity and degranulation. Hydrogen peroxide, the result of cellular oxidative activity, is produced primarily at the phagosomal membrane and within the phagosome. Moreover, the activity of the enzyme responsible for hydrogen peroxide production is enhanced by Ca^{2+} (12). The primary target for degranulation is also the phagosome, and free Ca^{2+} plays an important role in degranulation (13). Table 1C shows the mean $[Ca^{2+}]_i$ of neutrophils ingesting opsonized zymosan particles. The $[Ca^{2+}]_i$ increased significantly in the pseudopods (19.2 ± 9.9 nM) and in the periphagosomal cytoplasm (55.2 ± 28.5 nM) relative to the cell body. A neutrophil ingesting an opsonized zymosan particle is shown in Fig. 1, G through I. The regions of highest $[Ca^{2+}]_i$ are the pseudopods and the base of the developing phagosome. A neutrophil at a later stage of phagocytosis with a group of zymosan particles in the phagosome is shown in Fig. 1, J through L; $[Ca^{2+}]_i$ was highest in the periphagosomal cytoplasm. Cockcroft *et al.* (14) have shown that degranulation can be stimulated by increasing $[Ca^{2+}]_i$ in neutrophils with ionomycin when Ca^{2+}_0 is present. Likewise, increasing $[Ca^{2+}]_0$ stimulated lysozyme release in cells made permeable with saponin (15). Alternatively, buffering $[Ca^{2+}]_i$ with high concentrations of intracellular Quin2 decreased phagocytosis in monocytes (16).

The absence of $[Ca^{2+}]_0$ inhibits but does not block orientation, movement, degranulation, phagocytosis, and post-phagocytic oxidative metabolism (3, 17). The increase in $[Ca^{2+}]_i$ with soluble stimuli is blunted by the absence of $[Ca^{2+}]_0$. In order to determine the role of $[Ca^{2+}]_0$ on these $[Ca^{2+}]_i$ patterns, we carried out similar experiments in the absence of $[Ca^{2+}]_0$ with 10 mM EGTA. Table 1D shows the mean $[Ca^{2+}]_i$ of neutrophils migrating toward opsonized zymosan particles. There was no measurable difference in $[Ca^{2+}]_i$ of the lamellipodium and cell body of chemotactic cells. Since neutrophils can mobilize $[Ca^{2+}]_i$ from intracellular stores when stimulated without $[Ca^{2+}]_0$ (17), one would expect similar regional differences in the $[Ca^{2+}]_i$ distribution as observed during chemotaxis with $[Ca^{2+}]_0$ present. However, with 10 mM EGTA and $[Ca^{2+}]_0 < 10$ nM, some internal Ca^{2+} associated with the cortical cytoplasm of neutrophils might have been removed. In the absence of $[Ca^{2+}]_0$, the $[Ca^{2+}]_i$ in the pseudopods was not higher than in the cell body of

Table 1. Intracellular free calcium concentrations (mean nM \pm standard error of the mean). Statistical analysis was performed with a paired *t* test, comparing either the lamellipodium, pseudopod, or periphagosomal cytoplasm to the cell body. **P* < 0.05. (A) Neutrophils loaded with Quin2 (0.875 nmol per 10^6 cells). The lamellipodium is defined as the front third of the cell and the cell body as the middle third. (B) Neutrophils analyzed were actively migrating toward opsonized zymosan, which was no farther than 10 μ m from the cell. (C) The pseudopods are defined as the arms surrounding the opsonized zymosan particle. The periphagosomal $[Ca^{2+}]_i$ values were obtained from within 3 μ m of the developing or completed phagosome. (D) Chemotaxis toward opsonized zymosan in the absence of $[Ca^{2+}]_0$. (E) Phagocytosis of opsonized zymosan in the absence of $[Ca^{2+}]_0$.

| System | Cell body | Lamellipodium | Pseudopods | Periphagosome | Difference \pm standard error (n) |
|-------------------------|-------------------------------|---------------|--------------|---------------|---|
| $[Ca^{2+}]_0 = 1 \mu M$ | | | | | |
| A. Unstimulated | 74 \pm 4 | 69 \pm 3 | | | 5.2 \pm 3.1 (17) |
| B. Chemotaxis | 108 \pm 42 | 146 \pm 44 | | | 37.8* \pm 16.0 (12) |
| C. Phagocytosis | { 95 \pm 22 106 \pm 23 | | 114 \pm 32 | 161 \pm 44 | 19.2* \pm 9.9 (23) 55.2* \pm 28.5 (31) |
| $[Ca^{2+}]_0 < 10$ nM | | | | | |
| D. Chemotaxis | 65 \pm 4 | 64 \pm 6 | | | 1.4 \pm 1.9 (5) |
| E. Phagocytosis | { 68 \pm 7 63 \pm 6 | | 62 \pm 9 | 70 \pm 6 | 5.1 \pm 3.4 (7) 6.4* \pm 2.4 (11) |

neutrophils ingesting zymosan particles. However, there was a small but significant increase in $[Ca^{2+}]_i$ in the periphagosomal cytoplasm of neutrophils ingesting opsonized zymosan in Ca^{2+} -free medium. It thus appears that, with opsonized zymosan as a stimulus, most of the increase in $[Ca^{2+}]_i$ observed in the lamellipodium, pseudopods, and periphagosomal cytoplasm is from extracellular sources. The fact that these cells exhibited orientation, locomotion, and phagocytosis, albeit slowly, suggests that the changes in $[Ca^{2+}]_i$ were too small to detect.

The increases in $[Ca^{2+}]_i$ with these Quin2-loaded neutrophils is lower than the peak $[Ca^{2+}]_i$ reported for cell populations by others (18). Using neutrophils loaded with low concentrations of Quin2, Lew *et al.* (19) have shown that $[Ca^{2+}]_i$ increases to micromolar levels after stimulation with soluble stimuli; however, with high intracellular concentrations of Quin2 (0.9 nmol per 10^6 cells), the $[Ca^{2+}]_i$ reaches only 300 nM. Our estimated level of intracellular Quin2 was 0.875 nmol per 10^6 cells (20). In addition, our technique excludes the contribution of damaged cells, Quin2 leakage from loaded cells, and neutrophils with large Quin2 ester precipitates, all of which could elevate estimates of $[Ca^{2+}]_i$. Our technique averages eight frames (about 0.25 second), and thus a very transient peak could be blunted. Kruskal *et al.* (8), using single cell measurements in pituitary cells, found $[Ca^{2+}]_i$ in the same range as reported here for neutrophils.

The message that translates cell surface stimulation to an orchestration of host cellular responses is beginning to be understood. Changes in $[Ca^{2+}]_i$ modu-

late certain cellular responses such as oxidative activity, phagocytosis, locomotion, and degranulation. Regional increases in $[Ca^{2+}]_i$ occur during migration toward, and phagocytosis of, particulate stimuli. These regional changes in $[Ca^{2+}]_i$ occur at sites within the cell where important cellular functions take place. High regional $[Ca^{2+}]_i$ appears to be important for neutrophil functions such as directed movement, oxidative metabolism, and degranulation. Future studies are required to document the temporal sequences of these $[Ca^{2+}]_i$ patterns.

References and Notes

1. R. Snyderman and E. J. Goetzl, *Science* **213**, 830 (1981); J. I. Gallin and A. S. Rosenthal, *J. Cell Biol.* **62**, 594 (1974).
2. T. P. Stossel, *J. Cell Biol.* **58**, 346 (1973).
3. J. E. Smolen, H. M. Korchak, G. Weissmann, *Biochim. Biophys. Acta* **677**, 512 (1981).
4. R. Y. Tsien and T. J. Rink, *J. Cell Biol.* **94**, 325 (1982).
5. A. Boyum, *Scand. J. Clin. Lab. Invest.* **21** (Suppl. 97), 77 (1968).
6. Zymosan (1 mg) was suspended in 1 ml of fresh serum and agitated at 37°C for 30 minutes. The zymosan particles were washed twice with HBSS or twice with Ca^{2+} - and Mg^{2+} -free HBSS + 10 mM EGTA for experiments without $[Ca^{2+}]_0$; 10 μ l of the zymosan suspension was mixed with 10^6 neutrophils that had previously been attached to a cover slip.
7. J. Browne, P. McCourt, C. R. Somerville, *Science* **227**, 766 (1985).
8. B. A. Kruskal, C. H. Keith, F. R. Maxfield, *J. Cell Biol.* **99**, 1167 (1984).
9. To estimate $[Ca^{2+}]_i$ from the fluorescence intensity at 340 nm to that at 360 nm (I_{340}/I_{360}), we constructed a curve relating I_{340}/I_{360} to $[Ca^{2+}]_i$ using the computerized image analysis described in the text. EGTA-buffered solutions were prepared as previously described (8). Standard solutions of free calcium were based on the dissociation constant of calcium-Quin2 of 180 nM at 23°C and pH 7.05 (8). Standard solutions were prepared by the addition of 4.9 μ l of 0.372M Ca EGTA (determined by atomic absorption spectrometry) to 1 ml of the calibration buffer for 50 nM $[Ca^{2+}]_i$; 5 mM Quin2, 1.56 mM EGTA, 115 mM KCl, 20 mM NaCl, 10 mM MOPS, [2-(N-morpholino)ethanesulfonic acid], titrated to pH 7.05 with KOH.
10. J. A. Sullivan and G. L. Mandell, *Cell Motility* **3**, 31 (1983); N. H. Valerius, O. Stendahl, J. H. Hartwig, T. P. Stossel, *Cell* **24**, 195 (1981).
11. T. P. Stossel, J. H. Hartwig, H. L. Yin, F. S. Southwick, K. S. Zaner, *Fed. Proc. Fed. Am. Soc. Exp. Biol.* **43**, 2760 (1984).

12. R. A. Salata, J. A. Sullivan, G. L. Mandell, *Trans. Assoc. Am. Phys.* **97**, 375 (1984); H. Suzuki, M. J. Pabst, R. B. Johnston, Jr., *J. Biol. Chem.* **260**, 3635 (1985).
13. L. M. Goldstein, J. K. Horn, H. B. Kaplan, G. Weissman, *Biochem. Biophys. Res. Commun.* **60**, 807 (1974).
14. S. Cockroft, J. P. Bennet, B. D. Gomperts, *Biochem. J.* **200**, 501 (1981).
15. J. E. Smolen and S. J. Stoehr, *J. Immunol.* **134**, 1857 (1985).
16. J. D. E. Young, S. S. Ko, Z. A. Cohn, *Proc. Natl. Acad. Sci. U.S.A.* **81**, 5430 (1984).
17. M. B. Hallet and A. K. Campbell, *Cell Calcium* **5**, 1 (1984); T. P. Pozzan, P. D. Lew, C. B. Wollheim, R. Y. Tsien, *Science* **221**, 1413 (1983).
18. J. R. White, P. H. Naccache, T. F. P. Molski, P. Borgeat, R. I. Sha'afi, *Biochem. Biophys. Res. Commun.* **113**, 44 (1983).
19. P. D. Lew, C. B. Wollheim, F. A. Waldvogel, T. Pozzan, *J. Cell Biol.* **99**, 1212 (1984).
20. Quin2 was dissolved in 1.56 mM EGTA, 115 mM KCl, 20 mM NaCl, and 10 mM MOPS and titrated to pH 7.05 with KOH. We measured the fluorescence of Quin2 concentrations ranging from 50 μ M to 10 mM without calcium present by using the method described in the text. Quin2 concentrations of 2.5 mM approximated the fluorescence intensity of Quin2-loaded cells when excited by 360-nm light. Given a volume of free water of 0.35 μ l per 10^6 cells, this corresponds to an intracellular Quin2 concentration of 0.875 nmol per 10^6 cells.
21. We thank G. Sullivan for advice on the preparation of this manuscript. Supported by grants AI09504 and T32AI07046 from the National Institute of Allergy and Infectious Diseases.

29 May 1985; accepted 27 August 1985

High-Frequency Switching of Colony Morphology in *Candida albicans*

Abstract. *The pathogenic yeast Candida albicans switches heritably and at high frequency between at least seven general phenotypes identified by colony morphology on agar. Spontaneous conversion from the original smooth to variant phenotypes (star, ring, irregular wrinkle, hat, stipple, and fuzzy) occurs at a combined frequency of 1.4×10^{-4} , but is increased 200 times by a low dose of ultraviolet light that kills less than 10 percent of the cells. After the initial conversion, cells switch spontaneously to other phenotypes at a combined frequency of 2×10^{-2} . Switching is therefore heritable, but also reversible at high frequency. The genetic basis of this newly discovered process and its possible role in Candida pathogenesis are considered.*

BERNICE SLUTSKY

JEFFREY BUFFO

DAVID R. SOLL

Department of Biology,
University of Iowa,
Iowa City 52242

The dimorphic yeast *Candida albicans* is one of the most pervasive fungal pathogens in man (1). Although it has been assumed that its pathogenicity depends to a large extent on its capacity to grow in either a budding or hyphal form, this single developmental characteristic has never seemed to be sufficient to account for its capacity to invade so many diverse body locations, in many instances to evade antibiotic treatment (2) and the immune system (3), and to opportunistically infect a diverse spectrum of compromised hosts (4). In addition,

it has been shown that *C. albicans* is a diploid (5) with balanced lethals (6) and therefore most likely without a sexual phase or meiotic cycle. Where, then, does *C. albicans* obtain the diversity that appears to be basic to its success? The answer to this question may lie in the discovery that *C. albicans* spontaneously and reversibly switches at high frequency between at least seven general phenotypes that can be distinguished by a simple agar assay for colony morphology.

When clonal colonies of a standard strain of *Candida albicans* (3153A) were grown on an amino acid-rich agar (7) at 24°C for 7 days, the colony morphology was "smooth" (Fig. 1A). Smooth colonies exhibited an unmottled, or unwrinkled, surface, with no aerial mycelia. Cells removed from the surface of a

smooth colony were exclusively in the budding form of growth. On the underside of a mature colony, at the colony-agar interphase, hyphae penetrated the agar. Because of its smooth colony morphology, we will refer to the original parent strain as "original smooth" or "o-smooth."

When large numbers of cells of o-smooth were plated as clones, variant colony morphologies appeared spontaneously at a frequency of 1.4×10^{-4} . In 50,500 colonies examined, we found seven variant colonies: two "star" (Fig. 1B), three "ring" (Fig. 1C), and two "irregular wrinkle" (Fig. 1D). Colonies with the star morphology exhibited a slightly thickened perimeter encompassing a star with between 8 and 12 arms projecting peripherally and equidistant from one another (Fig. 1B). The arms usually did not connect centripetally, and their peripheral tips extended off the colony proper. Colonies with the ring morphology exhibited a very thick perimeter, encompassing up to one-third of their radius (Fig. 1C). The center of a ring colony was relatively thin in comparison, and was usually mottled in texture. Colonies with the irregular wrinkle morphology exhibited deep wrinkling throughout their surface (Fig. 1D). In contrast to o-smooth colonies, cells removed from the surface of star, ring, and irregular wrinkle colonies exhibited both budding and hyphal phenotypes. When original isolates of the three spontaneous variant morphologies were in turn plated as clones, the respective variant phenotype persisted in the majority of offspring. These phenotypes persisted in successive clonal platings.

When cells of o-smooth were plated as clones on agar and immediately treated with low doses of ultraviolet light, resulting in relatively low levels of cell death, variant colony morphologies appeared with even higher frequencies. At an ultraviolet light dose that killed only 8 percent of the cells, 136 out of the 5600 surviving clones exhibited variant colony morphologies, a combined frequency

Table 1. The frequency of variants in an ultraviolet-induced star colony emanating from original smooth and in ring, stipple, fuzzy, and r-smooth colonies emanating from the star.

| Switch phenotype | Number of clones | Number of colonies | Total switch colonies | Frequency of individual switch phenotypes | | | | | | Combined frequency of switching |
|------------------|------------------|--------------------|-----------------------|---|----------------------|----------------------|----------------------|----------------------|----------------------|---------------------------------|
| | | | | Star | Ring | Irregular wrinkle | Stipple | Fuzzy | r-Smooth | |
| Star | 1 | 25,000 | 442 | | | | | | | |
| Ring | 10 | 57,000 | 1,398 | 1.0×10^{-2} | 7.4×10^{-3} | 2.0×10^{-4} | 4.1×10^{-3} | 6.4×10^{-4} | 5.2×10^{-3} | 1.8×10^{-2} |
| Stipple | 6 | 36,100 | 3,933 | 7.8×10^{-3} | 2.9×10^{-3} | 1.0×10^{-3} | 4.7×10^{-4} | 2.6×10^{-4} | 9.8×10^{-3} | 2.5×10^{-2} |
| Fuzzy | 4 | 25,400 | 665 | 2.2×10^{-3} | 8.3×10^{-3} | 7.1×10^{-3} | | 2.4×10^{-3} | 6.1×10^{-3} | 1.1×10^{-1} |
| r-Smooth | 5 | 30,700 | 444 | 6.6×10^{-3} | 6.3×10^{-3} | 5.1×10^{-3} | 1.3×10^{-3} | | 9.4×10^{-3} | 2.6×10^{-2} |
| | | | | | | 1.2×10^{-3} | 2.9×10^{-4} | | | 1.4×10^{-2} |